



**AAS 01-026**

## Rocket Sled Testing of a Prototype Terrain-Relative Navigation System

Eli David Skulsky, Andrew Edie Johnson, Jeff Umland, Curtis Padgett, Bill Martin,  
Stacy Weinstein, Mark Wallace, Adam Steltzner, and Sam Thurman

Jet Propulsion Laboratory  
California Institute of Technology

---

### 24th ANNUAL AAS GUIDANCE AND CONTROL CONFERENCE

---

January 31 - February 4, 2001  
Breckenridge, Colorado

Sponsored by  
Rocky Mountain Section



AAS Publications Office, P.O. Box 28130 - San Diego, California 92198

## ROCKET SLED TESTING OF A PROTOTYPE TERRAIN-RELATIVE NAVIGATION SYSTEM

**Eli David Skulsky, Andrew Edie Johnson, Jeff Umland,  
Curtis Padgett, Bill Martin, Stacy Weinstein,  
Mark Wallace, Adam Steltzner, and Sam Thurman\***

The next generation of Martian landers (2007 and beyond) will employ a precision soft-landing capability that will make it possible to explore previously inaccessible regions on the surface of Mars. This capability will be enabled by onboard systems that automatically identify and avoid terrain containing steep slopes or rocks exceeding a particular terrain height. JPL is currently developing such a hazard detection and avoidance system; this system will map the landing zone with a scanning laser radar, identify hazards, select a safe landing zone, and then guide the vehicle to the selected landing area. This paper describes how one component of this system—hazard detection—is being tested using a rocket sled and simulated Martian terrain.

### INTRODUCTION

Landing sites for past missions to Mars have, for the most part, been located in relatively benign terrain. The need to avoid rocky or sloped areas was due to the inaccuracy of the guidance system and to the inability of the landing system to accommodate such features. Landing accuracy of better than 100 km was difficult to achieve and landing systems employed by vehicles such as Pathfinder were unable to accommodate large hazards or significant surface roughness<sup>1</sup>. However, recent discoveries of exposed sedimentary rocks<sup>2</sup> and possible near-surface water in the proximity of canyon walls<sup>3</sup> have increased the desire of scientists to explore more complicated terrain on the surface of Mars. Landing safely in close proximity to hazardous terrain necessitates improved landing vehicle accuracy and robustness.

---

\* All authors except Bill Martin are with the Jet Propulsion Laboratory, California Institute of Technology. Bill Martin is with the Naval Air Warfare Center, China Lake. All correspondence should be sent to Eli David Skulsky, Jet Propulsion Laboratory, 4800 Oak Grove Drive, M/S 198-219, Pasadena, CA 91109, e-mail: eli.d.skulsky@jpl.nasa.gov.

The next generation of Martian landers (2007 and beyond) will employ a precision soft-landing capability which will enable exploration of areas such as those described in references 2 and 3. The technology includes a fully autonomous onboard system that automatically identifies and avoids hazardous features such as steep slopes and large rocks. A system under development at the Jet Propulsion Laboratory (JPL) will map the landing zone, identify hazards, and guide the vehicle to a safe landing site, all during the terminal descent phase. This paper describes how one part of that system—hazard detection—is being tested.

The prototype JPL hazard detection system consists of a scanning laser radar (LIDAR), inertial measurement unit (IMU), and hazard detection and avoidance algorithms. The LIDAR performs a raster scan of the landing zone and data from the IMU is used to compensate for rotational and translational motion during the scan. The hazard detection algorithms construct a topographic map of the area using the motion-compensated LIDAR data and generate estimates of surface slope and roughness. These estimates are subsequently used to identify areas that exceed landing constraints dictated by vehicle design. The hazard detection software then selects a safe landing site, and this location is provided to the guidance algorithms, which then steer the vehicle to the selected location.

To test the hazard detection algorithms with real sensor data collected at typical descent speeds, a prototype LIDAR and commercial IMU will be mounted on a rocket sled. The sled will be accelerated to approximately 75 m/sec using a single solid rocket motor that is attached to a pusher sled in the rear. Measurements begin roughly 500 m in front of the target and continue until the sled passes the target. The on-board sensors will be mounted to an optical bench that is secured to the sled via a passive vibration isolation system designed and built at JPL.

Ground truth position and attitude information will be provided by independent sensor measurements from high speed film cameras, a laser range finder, and “screen boxes” which, when cut by sled-mounted knives, close an electrical circuit to provide sled position with respect to the sled track. All sensor data will be time-tagged and stored on board in real-time using two ruggedized field computers. The target consists of a set of hemispheres of various radii mounted to a wall of stacked sea vans (12 m × 65 m) placed on the side of the track. Using the surveyed positions and radii of each hemisphere, a ground truth model of the target will be generated; this model will be used to verify the output of the surface reconstruction and hazard detection algorithms.

### **Why a rocket sled?**

A rocket sled was chosen to carry the LIDAR and associated instrumentation for the following reasons: high-speed, repeatability, safety, and existing test infrastructure. To convincingly demonstrate that the hazard detection technology under development at JPL meets mission requirements, we wish to test the system under conditions that are as realistic as possible but which do not jeopardize the equipment. To this end, a large area

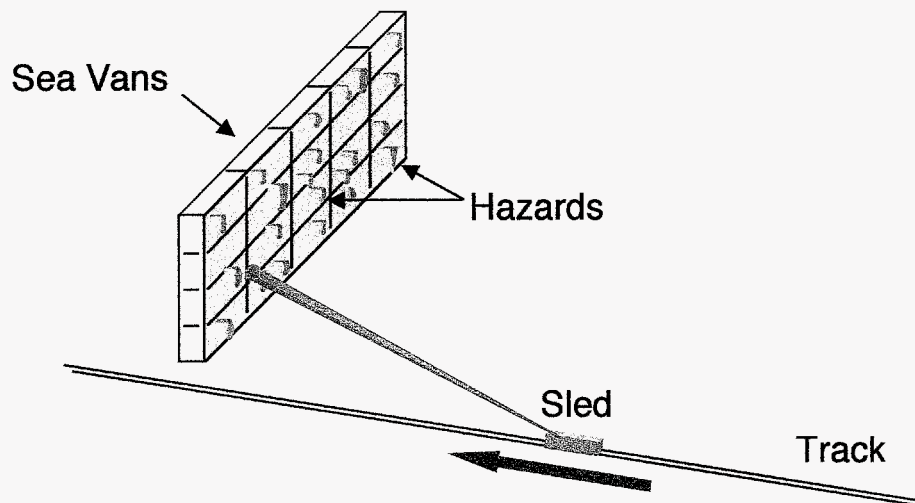
is required to allow relatively high-speed (> 50 m/sec) motion and to accommodate a large, simulated Martian terrain. Furthermore, the LIDAR beam is hazardous to the eye so the tests must be performed in an area which is isolated from the public. The Supersonic Naval Ordnance Research Track (SNORT) at the Naval Air Warfare Center (NAWC) easily meets both requirements. SNORT also provides a level of test repeatability which is especially valuable for technology demonstrations of this nature.

## TEST OBJECTIVES

The objectives of the test are threefold:

- Demonstrate that a LIDAR-based system, traveling at typical Mars descent speeds, can build a terrain map that can be used for hazard detection and terminal guidance during the descent phase of a Mars lander mission.
- Demonstrate that the hazard detection and terminal guidance algorithms and software function with the sensor data as generated.
- Develop a test approach and infrastructure for terrain sensing and instrument ground truth.

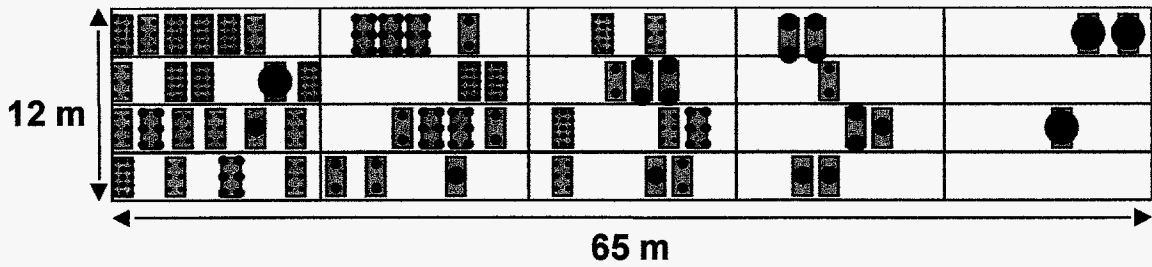
## SLED TEST OVERVIEW



**Figure 1 LIDAR scanning as the sled travels along the track.**

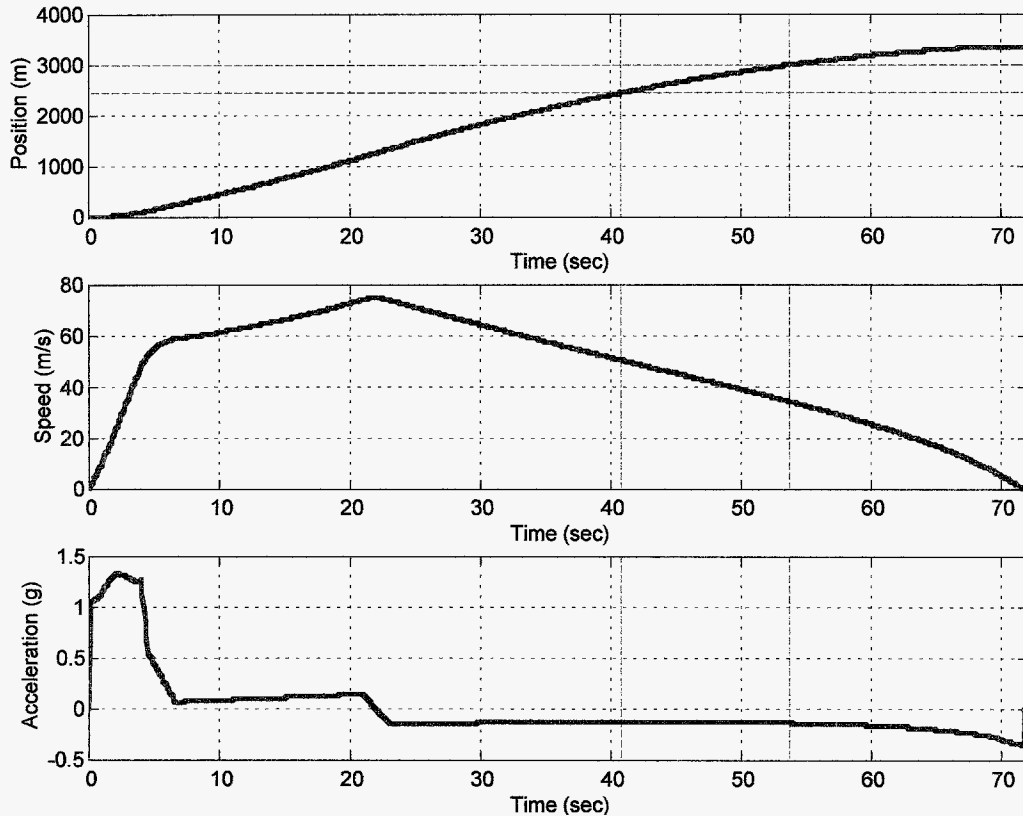
The sled test consists of an instrumented rocket sled that travels along a track propelled by a solid rocket motor. The tests are performed at the Supersonic Naval Ordnance Research Track (SNORT) at the Naval Air Warfare Center in China Lake, California. SNORT is a dual rail, 6500 m long track that is capable of handling speeds in excess of mach 4. On one side of the track at the 3000 m point is a simulated Martian terrain constructed on a set of stacked sea vans approximately 12 m x 65 m in size (Figure 1 and

Figure 2). Sea vans provide an inexpensive but sturdy structure on which to temporarily place the simulated Martian terrain.



**Figure 2 Hemispheres as targets mounted to the side of a wall of sea vans.**

For the first tests, the Martian terrain will be represented by a set of hemispheres of varying diameter and known location. The hemispheres will be mounted to plywood boards that are hung on the side of the sea vans (Figure 2); the boards are used to facilitate target construction and surveying. Hemispheres were selected for the early tests to facilitate post-test analysis; after surveying the position of the hemispheres on the target, a CAD model can be constructed from which true target shape can be extracted. In future tests the hemispheres will be replaced with more realistic terrain (rocks, local slopes, etc.).



**Figure 3 Rocket Sled Trajectory. The dashed red lines indicate the beginning and end of the experiment phase of a run (between 2500 m and 3000 m).**

The rocket sled used for this experiment was built in the late 1950s to test the Polaris Inertial Guidance system (thus the name: PIG sled). The PIG sled is propelled for a short time by a large solid rocket motor mounted to a pusher sled in the rear. In our experiment, the PIG sled is accelerated to approximately 75 m/sec at a relatively gentle peak acceleration of about 1.3 g. The motor burns out approximately 23 sec after ignition and the sled coasts to a stop 49 sec later (Figure 3).

Since the prototype LIDAR used in this experiment has a range of about 500 m, the trajectory was designed so that the sled speed 500 m from the target is between 50 m/sec and 100 m/sec, typical descent speeds during the terminal phase of landing on Mars.

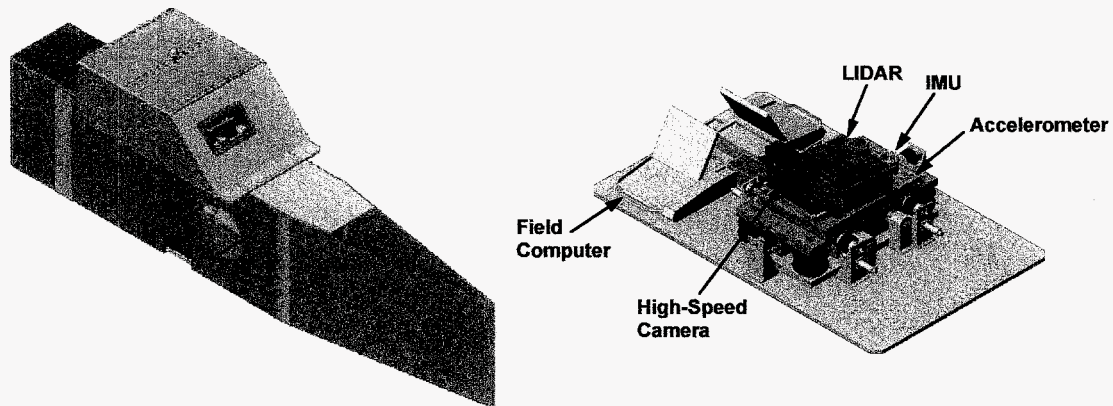


**Figure 4** The Instrument Pallet and Canopy atop the Polaris Inertial Guidance (PIG) Sled are shown on the left. The diagram on the right shows the high-speed camera, LIDAR, IMU, and accelerometers mounted on the passive vibration isolation system.

The instrumentation consists of a set of “flight-like” sensors (LIDAR, IMU) and “truth” sensors (accelerometers, high-speed camera, laser distance meter, screen boxes) from which data is captured and post-processed. The flight-like sensors, high-speed camera and the accelerometers are mounted to a passive vibration isolation system that sits on top of the rocket sled (Figure 4). The rocket sled also carries computers for data collection and time-tagging as well as a self-contained power system.

### **Flight-Like Sensors**

The two “flight-like” sensors—the IMU and the LIDAR—functionally resemble the sensors that will be used in the flight system, but the actual components for the flight system have not been selected. For the tests we will use a Litton LN-200 Inertial Measurement Unit and the Optech Laser Ranging Instrument (LRI).

The LN-200 IMU consists of three orthogonal fiber-optic gyros and three orthogonal silicon accelerometers in a package that is roughly the size of a coffee mug. The LN-200 is configured to provide 400 samples per second (angular velocity and acceleration counts) via an RS-485 serial interface.

The Optech LRI (Figure 5) incorporates an infrared (1064 nm) laser radar and two scanning mirrors to capture three-dimensional shape data. The LRI has a pulse repetition frequency (PRF) of 8 KHz, a maximum field of view of  $10^{\circ} \times 10^{\circ}$  with a maximum resolution of  $500 \times 1000$  samples, a maximum range of 500 m, and 2 mrad beam divergence. For the sled tests, a  $5^{\circ} \times 10^{\circ}$  and  $50 \times 100$  sample scan pattern will be employed; this scan pattern will provide 10 to 15 scans of the target during each test. Range and angle measurements from the LRI are collected by a dedicated computer while timing data is collected by the same onboard field computer which collects the IMU, accelerometer, and screen box data.

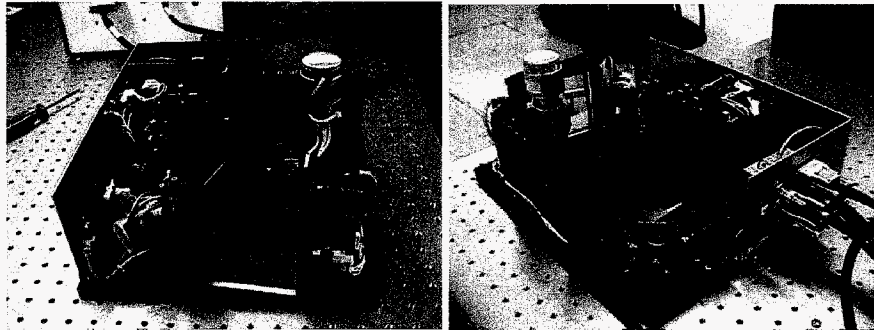


**Figure 5 Front and rear views of the Optech Laser Rangefinding Instrument (LRI)**

### **Truth Sensors**

Measurements from the truth sensors are used to generate a high accuracy estimate of the sled trajectory that is completely independent of the flight sensor measurements. The truth sensors consist of a high-speed film camera, six QA-2000 Q-flex accelerometers, a laser distance meter, and a set of screen boxes. The camera and the accelerometers are mounted on the optical bench; the laser distance meter and the screen boxes are fixed to the side of the track.

The high-speed film camera is used to obtain the sled attitude with respect to the target. The camera, which operates at 250 frames per second, captures images of a set of surveyed lights on the target. The camera is pin-registered to eliminate vertical and horizontal synchronization problems and encodes a 100 Hz timing signal directly on the film. At 250 fps, the camera can capture 40 sec of test footage.

After the test is complete the film is analyzed to obtain the direction to the lights as seen by the camera. This is a time-consuming task requiring an analyst to manually identify and mark light positions that are recorded by a computer. Next, the light direction measurements are combined with measurements of the camera position and knowledge of the three-dimensional position of the lights to obtain estimates of the sled attitude versus time.

The QA-2000 Q-flex accelerometers serve two purposes: estimation of the sled position and estimation of the optical bench vibrational environment. Accelerometer data is collected and timetagged by the onboard field computer.

The laser distance meter (LDM), manufactured by Riegl USA, will be used to provide direct high-speed (2 KHz) measurements of the sled position. The LDM measurements—which are accurate to about 2.5 cm—will be collected by a computer and tagged with GPS time (the computer includes a GPS receiver). A retroreflector on the front of the sled increases the operating range of the LDM from 700 m to over 1000 m.

Several screen boxes on the side of the track provide absolute sled position measurements and are used as a flash trigger so that high-speed camera frames can be synchronized with GPS time.

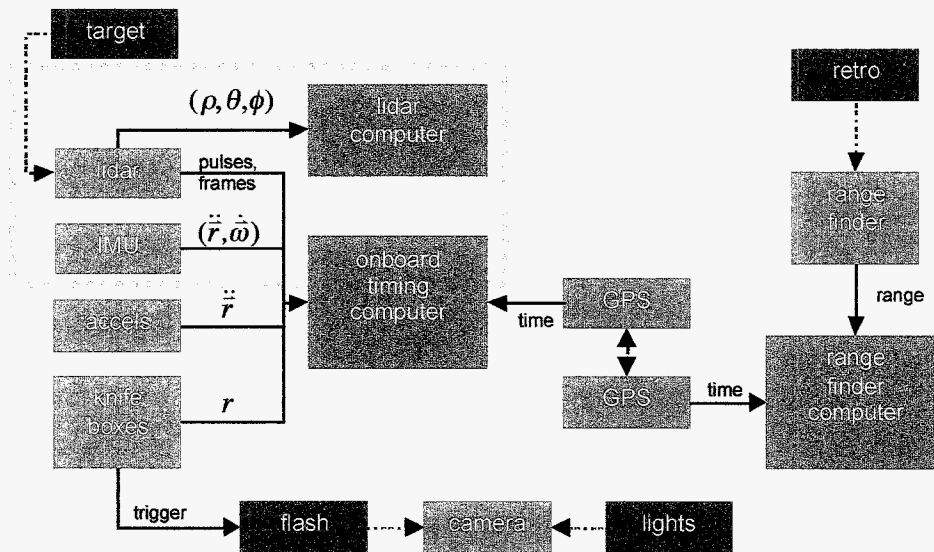


**Figure 6 Instrumentation Block Diagram**

Figure 6 shows how the measurements from each sensor are time-tagged and stored with consistent GPS time for post-test analysis.

## Vibration Isolation

A vibration isolation system was developed for the sled test to protect the LIDAR from the broadband random dynamic environment generated by the sled and solid rocket motor. The LIDAR rocket sled test vibration isolation hardware is shown in Figure 7. Conceptually, the vibration isolator is a two-stage system. The first stage consists of a 275 kg seismic mass supported vertically on four air springs. The seismic mass is constrained horizontally by an additional set of six air springs (these springs are not shown in Figure 7). The second stage consists of the optical bench, which when fully loaded with the LIDAR, high-speed camera, and IMU weighs 45 kg. The optical bench is supported on the seismic mass by four shock mounts that provide both in-plane and out-of-plane restraint. The natural frequencies of all six modes associated with the rigid body motion of the first stage of the isolation system range from 3 to 8 Hz. The natural frequencies associated with the second stage range from 20 to 30 Hz.

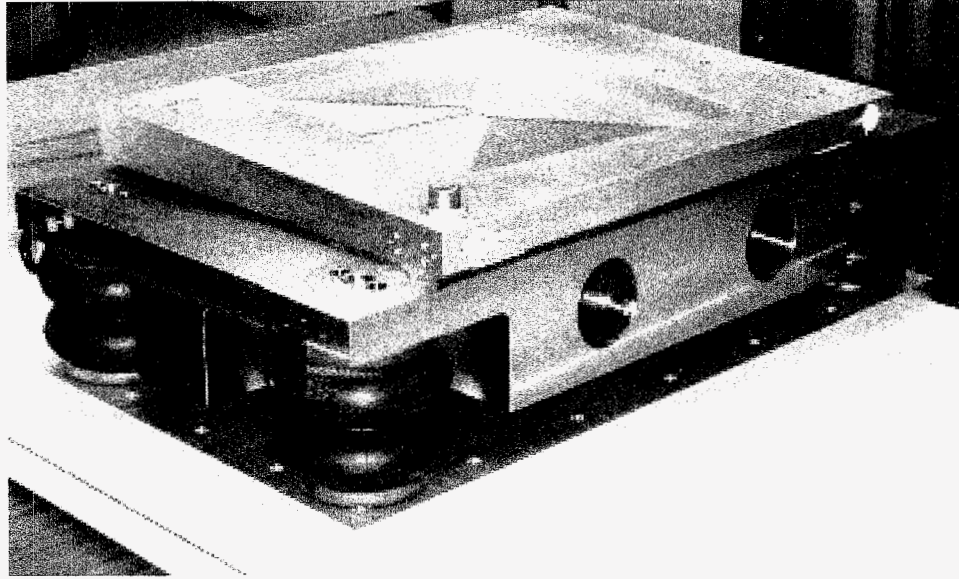


**Figure 7 Two-Stage Passive Vibration Isolation System**

## **Alignment**

Since LIDAR frames are not captured instantly (each frame requires about one second), motion compensation must be performed on each pixel of each frame before the hazard detection software can be run. Consequently, the rigid transformation between the LRI and the IMU must be known. Similarly, the orientation of the Q-flex accelerometers and high-speed camera must be known with respect to the LRI to validate the hazard detection results. We also need to know the location (but not the orientation) of the laser distance meter, screen boxes, and target lights. To this end, an alignment procedure was developed to determine the orientation and position of any instrument (as needed) with respect to any other instrument. The objectives of the alignment procedure are to determine the position and orientation of all sensors in the Master Reference Frame at all times and to determine the orientation of the IMU and Q-flex accelerometers in geocentric inertial (GCI) coordinates to compensate for Earth rotational motion and gravity.

Alongside the track are a set of permanent, surveyed, quarter-size “monuments” spaced roughly every meter. Because they are permanent and because their locations are known, two of these monuments (along with a third permanent off-track marker) will be used to construct a coordinate frame to which every instrument and target will be referenced. We call this coordinate frame the *Master Reference Frame* (MRF).

To obtain the transformation between an arbitrary coordinate frame (call it  $\mathcal{A}$ ) and the MRF, we use a total station surveying instrument (which provides the angles and range to a target) to measure the position in total station coordinates of the MRF monuments and the position in total station coordinates of the points which define  $\mathcal{A}$ . From there it is straightforward to construct the transformation between the MRF and  $\mathcal{A}$ . We do this for

every instrument and for every target. Furthermore, we measure the position (though not the orientation because we treat these as points) of the laser distance meter, the screen boxes, and the target lights.

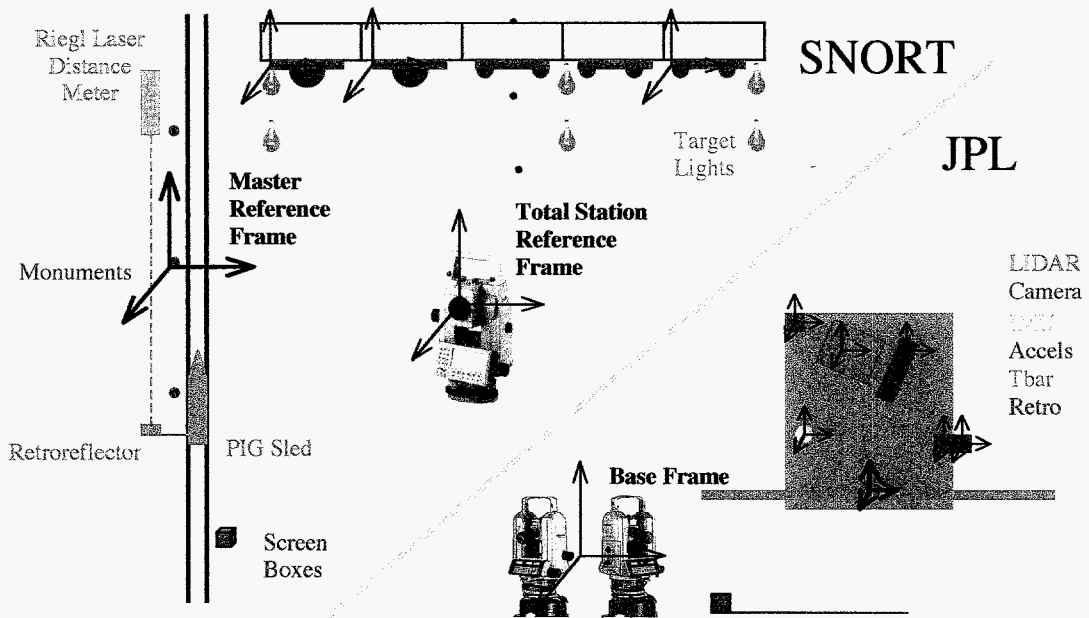


**Figure 8 Sled Test Alignment Diagram. Optical bench alignments will occur at JPL, while track alignments will occur at SNORT.**

A similar procedure is performed for the instruments on the optical bench. In this case, we measure the orientation of each instrument (LIDAR, IMU, accelerometers, high-speed camera) using a multiple theodolite system (MTS) in MTS coordinates; this step allows us to determine the orientation of any instrument with respect to the high-speed camera. Next, the high-speed camera is calibrated to correct for focal length and optical distortion. As described below, the attitude of the high-speed camera with respect to the target as the sled travels along the track can be determined by measuring the position of the target lights in the camera field of view. If the camera attitude is known and if the orientation of an instrument with respect to the camera is known, then we can determine the attitude of that instrument with respect to the target.

A final step in the alignment procedure is required to obtain the orientation of the IMU in geocentric inertial coordinates. This step is necessary to remove the biases introduced into IMU measurements by Earth rotation and gravity. Using a Differential GPS system and a total station this transformation can be computed by measuring the position of distant monuments in GPS and total station coordinates followed by a correction that maps geodetic to geocentric coordinates.



in the MRF is determined using the High Speed Camera (HSC) images of the target lights. Finally these measurements and the measurements from the Q-flex accelerometers are processed with a Kalman filter to obtain a high-accuracy truth trajectory.

Sled position is estimated from the LDM measurements as follows (Figure 10): The LDM provides a measurement of the range to a target along the line of sight; this measurement defines a sphere. By finding the intersection of this sphere with a piece-wise linear representation of the track, the position of the sled can be determined. Computing sled position in this way uses knowledge of the position of the LDM and the geometry of the sled track in the Master Reference Frame (MRF) obtained during pre-test surveying

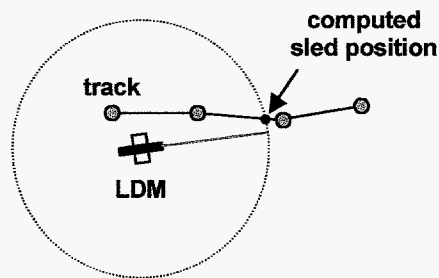


**Figure 10 Procedure for computing sled position from track survey and laser distance meter (LDM) measurements.**

Simulations have shown that the worst-case position error achieved through this technique is about 6 cm.

The truth sled attitude is computed for every image taken with the HSC using a nonlinear attitude estimation algorithm. The inputs to the algorithm are the known 3-D positions of target lights in the MRF, the 2-D image positions of each light in the image taken by the HSC and the position of the sled computed using the LDM. The output of the estimation procedure is the attitude and attitude covariance of the sled in the MRF. Simulations have shown this procedure to be accurate to 1 mrad.

The final step in truth trajectory generation is to combine the position and attitude measurements obtained with the LDM and HSC with high accuracy acceleration measurements taken with the Q-Flex accelerometers. These measurements are combined using a Kalman filter that integrates the accelerometer values given the attitude profile provided by the HSC attitude estimates. The LDM positions are then used as measurements in the filter to improve the accelerometer only trajectory. Error analysis gives a worst case error for the ground truth trajectory of 6 cm in position and 1 mrad in attitude.

## **Truth Shape Generation**

The ground truth shape of the target is generated through a combination of surveying and construction of the target to tolerance. The target is composed of multiple plywood boards onto which are attached acrylic hemispheres. The hemispheres are constructed with a known tolerance on hemisphere diameter. The hemispheres are then placed accurately on the each plywood board within a known tolerance to the corners of the board. After the boards are hung on the wall of sea vans, the position and attitude of each board is determined by surveying the corners of each board. Using these surveying measurements and parametric models of the hemispheres, a CAD model of the entire target surface is constructed. Concatenating all error sources results in a worst-case estimate of 3 cm in hemisphere position and 1 mrad error in board attitude.

## **Flight Trajectory Generation**

Integrating the IMU data generates the flight trajectory. Using a model of the LN-200 IMU, the 3-axis accelerations and the 3-axis angular rates are integrated simultaneously by a navigation filter to generate the position and attitude of the sled as a function of time. By combining this trajectory with sensor coordinate transformations and the initial starting position and attitude of the IMU (from ground truth measurement) the position and attitude of the sled is transformed into the MRF. The expected accuracy of the flight trajectory at the end of the test is 18 cm position error and 1.45 mrad attitude error. This relatively large position error will be reduced when LIDAR data is incorporated into the navigation filter.

## **Flight Shape Generation**

To generate the flight shape, each sample acquired by the LRI is placed in the MRF using the flight trajectory generated using the IMU. This process is called motion compensation. The expected errors on flight shape are 20 cm in position and 2 mrad in attitude.

## **Same Shape Test**

The first test of system performance is to compare the flight shape to the truth shape. The flight shape is a set of 3-D points in the MRF and the truth shape is a CAD model in the MRF. These two data sets can be compared as follows: for each LRI sample, find the distance to the closest point on the surface of the truth CAD model. This process can be sped up using efficient data structures and the parametric representation of the truth model. These distances can then be analyzed to determine global error statistics as well as local error maps. The same shape test will determine any deficiencies in the data collection system.

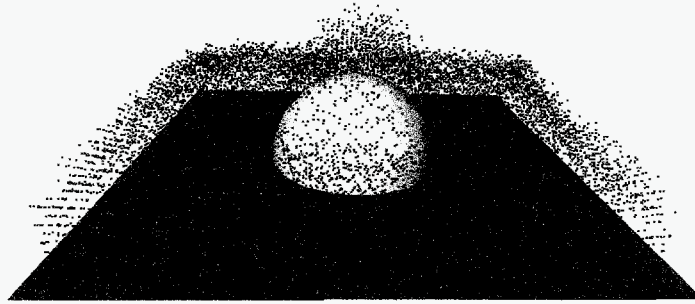


Figure 11 Example Alignment of a CAD target model (white) and 3-D lidar samples (blue).

### Same Hazards Test

The next test of system performance compares the hazards detected from the flight shape data to hazards extracted from the truth CAD model. A particular patch of terrain presents a hazard to the spacecraft during landing if the slope of the patch is too steep or the patch contains rocks or other protuberances that are taller than a certain terrain height. To quantitatively determine if a patch is hazardous, the slope and terrain variation over the patch must be measured. Our algorithms estimate the location of surface hazards given the motion compensated flight shape as follows<sup>6</sup>: First an elevation map is generated from the 3-D LIDAR samples. Next, estimates of local slope and roughness are computed over the entire elevation map. Finally, areas of the terrain map that exceed constraints on surface slope and roughness given the footprint of the lander are determined. Images of terrain, local slope, local roughness and detected hazards for a real LRI scan of a cliff at China Lake are given in Figure 12.

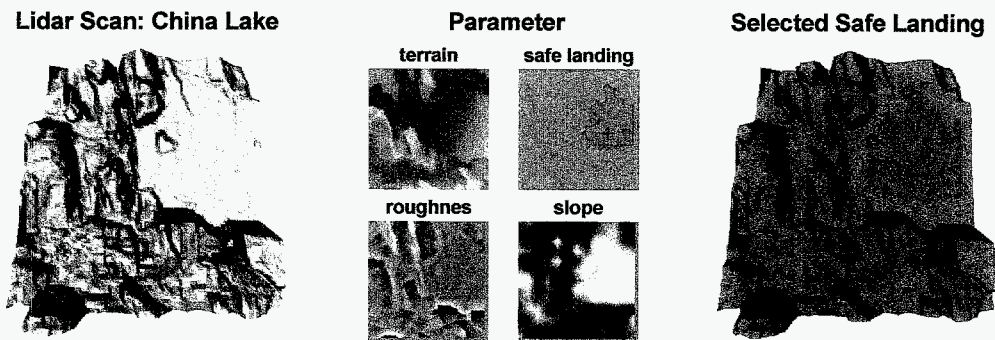


Figure 12 Hazard detection parameter maps applied to a stationary LRI scan of a cliff.

Truth hazards are extracted from the truth shape by generating a high resolution terrain map from the target CAD model and then estimating local slopes and roughness in the same way that they are estimated for the flight shape data. Our hazard detection test will compare the hazards detected in the flight data to the hazards extracted from the truth shape at various roughness and slope levels. If the flight data successfully detects all of

the hazards present in the target, then our hazard detection system concept will be validated. If some hazards are not detected, the test will be used to determine weak aspects of the system that will need to be improved in subsequent hazard detection systems.

### Same Trajectory Test

The final test of the system will compare the trajectory of the sled computed using flight sensors to the truth trajectory. Initially the trajectory computed from the IMU alone can be compared to the truth trajectory. We expect the IMU trajectory to have errors that are too large for precision landing. Fortunately the LRI data can be used to decrease these errors. As shown in Figure 13, by correlating terrain maps generated from LRI scans, an estimate of the sled motion relative to the target can be computed<sup>5</sup>. These motion estimates can be used to generate a trajectory for the sled that is more accurate than the IMU alone trajectory. The same trajectory test will be used to assess the performance of this and other LIDAR-based navigation algorithms.

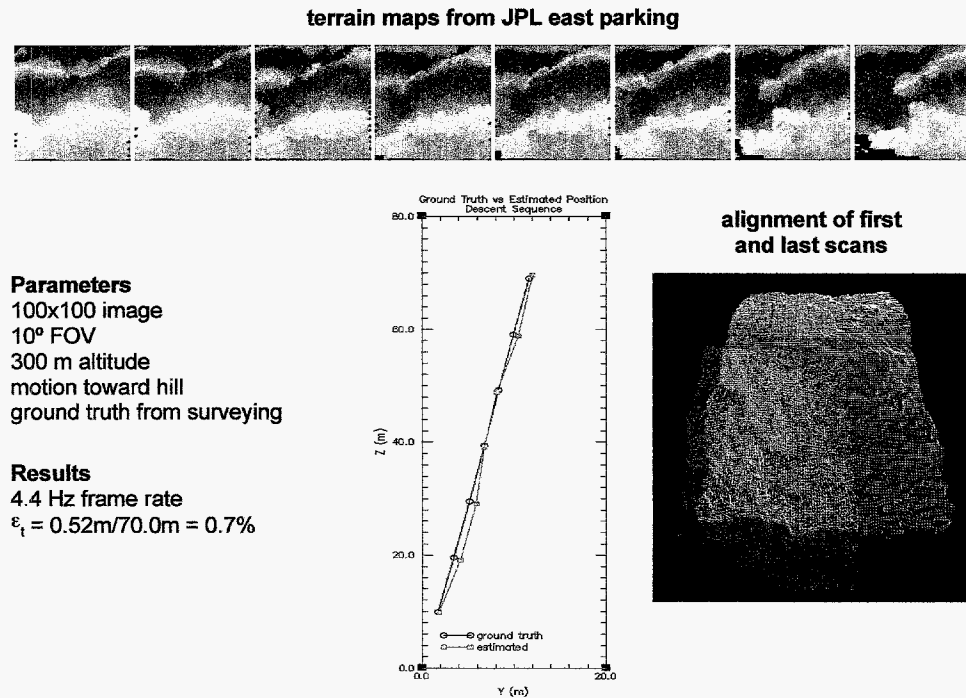


**Figure 13 Result of LIDAR-based motion estimation**

### CONCLUSION

An approach to testing a hazard detection system for landing on Mars was described. The approach provides a safe and repeatable means to demonstrate that hazard detection—a critical technology component of the next generation of Mars landers—is up to the task.

Future work in this area will include modifications to the LIDAR system to incorporate an external mirror for landing site tracking during landing as well as tests of different LIDARs and alternate sensors including a radar.

## **ACKNOWLEDGMENTS**

The authors would like to express our gratitude to Calvin Clayson, Dex Hansard, Mike Herr, and Lyndon Martinsen of Naval Air Warfare Center, China Lake for their invaluable experience and assistance in performing the rocket sled tests. We would also like to thank Bob Bishop at U.T. Austin and Tim Crain at Johnson Space Center as well as Dan Burkhart, Frank Loya, Jim Granger, David Rice, and Stephen Dawson--our colleagues at JPL.

This work was performed at the Jet Propulsion Laboratory, California Institute of Technology, under contract with the National Aeronautics and Space Administration.

## **References**

1. Golombek, M.P., Cook, R.A., et al, "Overview of the Mars Pathfinder Mission and Assessment of Landing Site Predictions," *Science*, December 5, 1997; 278: 1743-1748.
2. M.C. Malin and K.S. Edgett, "Sedimentary Rocks of Early Mars," *Science* 2000 December 8; 290:1927-1937.
3. M.C. Malin and K.S. Edgett, "Evidence for Recent Groundwater Seepage and Surface Runoff on Mars," *Science* 2000 June 30; 288: 2330-2335.
4. Johnson, A.E., Skulsky E.D., Loya, F., and Burkhart, D., *Mars Lander ATD Sled Test Software Review*, JPL Internal Document, December 7, 2000.
5. Johnson, A E., and San Martin, M., "Motion Estmation from Laser Ranging for Autonomous Comet Landing," *Proc. Int'l Conf. Robotics and Automation (ICRA '00)*, April 2000.
6. Johnson, A.E., Klumpp, A., Collier, J., and Wolf, A., "Lidar-Based Hazard Avoidance for Safe Landing on Mars," AAS/AIAA Space Flight Mechanic Meeting, (To Appear). February 2001.